Supporting Information

A bulky DNA lesion derived from a highly potent polycyclic aromatic tumorigen stabilizes nucleosome core particle structure

Yuqin Cai[a], Lihua Wang[a], Shuang Ding[a], Adam Schwaid[b], Nicholas E. Geacintov[b], and Suse Broyde[a,]*.

[a]Department of Biology and [b]Chemistry, New York University, New York, N.Y., 10003,

***Corresponding Author:** Suse Broyde, broyde@nyu.edu Tel. (212) 998-8231

Fax. (212) 995-4015

Running Title: structure of lesion-damaged nucleosome

Keywords: nucleosome core particle; lesion-damaged nucleosome; nucleotide excision repair; DNA-protein interactions; dibenzo[*a,l*]pyrene adenine adducts

Methods

Molecular modeling of the initial lesion-containing and unmodified NCP structure for MD simulations

Unmodified NCP Since our 14*S* (−)-*trans*-*anti*-DB[*a,l*]P-N^6-dA adduct adopts an intercalative conformation (see below), we used a nucleosome structure with naturally base-stretched segment of nucleosomal DNA (PDB (*1*) ID: 2NZD) (*2*) that can serve as an intercalation pocket upon alkylation by an aromatic chemical (*3*). The base sequence contexts around the intercalation pocket (at the 1.5 SHL, Figure 1d) was modified to the sequence context CAC:GTG (C202-A203-C204:G87-T88-G89) (Figure 1d), which has been extensively investigated (*4-9*).

Lesion-containing NCP Structural characterizations of *R* and *S* N^6-dA adducts derived from the planar bay region PAH B[*a*]P (Figure S1) (*10-16*), and the twisted fjord region PAH B[*c*]Ph (Figure S1) (*5, 6, 17*) and B[*g*]C (*8*) have been carried out by NMR methods and computational approaches. These studies have shown that the N^6-dA adducts adopt classical intercalation-type conformations: the *S* stereoisomers are intercalated on the 3'-side of the modified adenine, while the *R* stereoisomers are positioned on the 5'-side, and Watson-Crick base pairing, although distorted, remains at the damaged A:T pair. Accordingly, the initial

model for the 14*S* (−)-*trans-anti*-DB[*a,l*]P-N^6-dA adduct was built from the duplex 11-mer high resolution NMR solution structure of the fjord region B[*c*]Ph analog with the same stereochemistry at the linkage site, 1*S* (−)-*trans-anti*-B[*c*]Ph-N^6-dA (*6*) (Figure S1). Two rings were added to the B[*c*]Ph to create the DB[*a,l*]P initial model. This model on the nucleotide level was subjected to geometry optimization utilizing the Gaussian 03 package from Gaussian, Inc (*18*), and the optimized DB[*a,l*]P was relinked, with identical torsion angles, to the damaged adenine of the duplex 11-mer, and subjected to 30-ns of MD simulations (CaiY., Broyde S. et al, manuscript in preparation). Spectroscopic observations reveal that the UV absorption maximum for this adduct is red-shifted (Figure S2) which is fully consistent with an intercalative conformation.

Using the best representative structure (*19*) (shown in Figure 1b) from this ensemble, the lesion was cut (at the C14-N^6 bond (Figure S1)) and covalently linked to the adenine (A203) at the nucleosome stretch site (Figure 1d). The lesion-DNA linkage site torsion angles α' and β' assumed the same values as in the initial B[*c*]Ph adduct NMR structure (*6*) (α' = 130.6°, β' = 110.7°, Figure S1). Thus, we obtained a classical intercalation structure of the 14*S* (−)-*trans-anti*-DB[*a,l*]P-N^6-dA adduct covalently linked in the nucleosome stretch site, with the lesion occupying the intercalation pocket (Figures 1d and S3). Modeling software InsightII and Discovery Studio (Accelrys Inc.) were used.

Force field

The Cornell et al. force field (*20*) with modifications (*21, 22*) and the parm99 parameter set (*23*) modified by the parmbsc0 DNA parameters (*24*) were employed for all simulations.

Partial charges for the 14*S* (–)-*trans*-*anti*-DB[*a,l*]P-N^6-dA adduct were calculated on the nucleotide level for the initial models, using Hartree Fock quantum mechanical calculations with 6-31G* basis set without geometry optimization, employing the Gaussian 03 package from Gaussian, Inc (*18*). The charges were then fitted to each atomic center with the RESP algorithm (*25, 26*). The fitted charges are shown in Table S5. Missing bond and angle parameters were added to the force field by analogy to chemically similar atom types already exist in the parm99 parameter set and are shown in Table S6.

Protonation

The online protonation server PDB2PQR (http://pdb2pqr-1.wustl.edu/pdb2pqr/) (*27, 28*) was employed to determine the protonation state of the amino acid side chains. Based on the results of the PDB2PQR calculation, together with close inspection of the surrounding environment for possible hydrogen bonds, the ionization state of acids and bases in HIS, ARG, LYS, GLU and ASP were manually assigned. In our case, only HIS amino acids need to be assigned since the protonation state of a histidine is not clear from the crystal structure. The HIS can be protonated either on the $N^{\delta 1}$ or $N^{\varepsilon 2}$ or both to produce HID, HIE, and HIP, respectively. A HIS residue must be the HID type to accept a hydrogen bond, whereas it must be either HIE or HIP to donate a hydrogen bond. The decision to choose between an HIE and an HIP was made based on the availability of an acceptor in the proximity. The results are: HIE: 487, 538, 746, 923; HIP: 594, 654, 979; HID: 627, 672, 770, 827, 872, 1012, 1039.

MD protocols

The AMBER 9.0 simulation package (*29*) was utilized to carry out all minimization and MD simulations. The LEaP module was used to add hydrogen atoms and neutralize the system with K^+ counterions. Hydrogen atoms of the nucleosome core particle were minimized for 600 steps of steepest-descent followed by 600 steps of conjugate gradient. In this minimization, an implicit solvent model was used with a distance-dependent dielectric function of $\varepsilon = 4.0r$, with r being the distance between two atoms. The systems were then reoriented using SIMULAID (*30*) to minimize the number of water molecules needed to solvate the system. A periodic rectangular box of TIP3P water (*31*) with 10.0 Å buffer was created around the NCPs with the LEaP module. For the unmodified NCP, the box dimensions were approximately 136 Å x 142 Å x 94 Å, with a total of ~41571 water molecules. For the 14*S* (–)-*trans*-*anti*-DB[*a,l*]P-N^6-dA adduct-containing NCP, the box dimensions were approximately 136 Å x 142 Å x 94 Å, with a total of ~41563 water molecules.

The following minimization, heating, MD equilibration and production protocols were utilized. To begin with, the counterions and water molecules were minimized for 2500 steps of steepest descent and 2500 steps of conjugate gradient, with 50 kcal/mol restraints on the solute atoms. Then, 30 ps initial MD at 10K with 25 kcal/mol restraints on solute were performed to allow the solvent to relax. Next, the system was heated up from 10K to 300K at constant volume over 30 ps with 10 kcal/mol restraint on the NCP. The restraints on the solute were relaxed from 10 kcal/mol (for 30 ps) to 1 kcal/mol (for 40 ps) to 0.1 kcal/mol (50 ps). Subsequently, production MD was conducted at 1 atm, 300K for 65 ns, with 1 ps coupling constant for both pressure and temperature. These simulation protocols are similar to those given in earlier publication from our group (*32*).

In all MD simulations, the Particle-Mesh Ewald (*33, 34*) method with 9.0 Å cutoff for the non-bonded interactions was used. A 2.0 fs time step and the SHAKE algorithm (*35*) were applied in the MD simulations. All other parameters were default values in the AMBER 9 simulation package.

The stability of the MD simulation was evaluated. For each system, the root mean square deviation (RMSD) of each snapshot in the trajectory relative to its respective initial structure was plotted as a function of time and is shown in Figure S5. RMSDs for the local region (within 15 Å to the damaged base A203*) of the damaged residue and its undamaged counterpart (within 15 Å to the base A203) of each snapshot in the trajectory relative to its respective initial structure were plotted as a function of time and are also shown (Figure 3d). For both cases, the MD achieved stability, fluctuating around the mean after 20.0 ns of simulation, and we employed the structural ensembles from the 20 – 65.0 ns time frame at 10 ps intervals for further analyses.

Structural analyses

The PTRAJ module of the AMBER 9 package (*29*) was employed for structural analyses. The CARNAL module of the AMBER 7 package (*36*) was utilized to compute hydrogen bond occupancies. Frames were selected at 10 ps intervals from the last 45.0 ns of simulation. The DNA duplex helicoidal parameters and groove dimensions were analyzed using MD Toolchest (*37, 38*); for the groove dimensions, 5.8 Å was subtracted from the pairwise phosphorous-phosphorous distances to account for the van der Waals radius of the P atoms (*39*). Van der Waals interaction energies for the damaged NCP at the intercalation

pocket were computed between the DB[*a,l*]P aromatic rings and the adjacent bases, namely, T88, A203, C87, and G204. For the unmodified NCP, the interaction energies between the same base pairs that form the intercalation pocket were computed for comparison. The ANAL module of the AMBER 9 package (*29*) was used for these computations. The best representative structures (*19*) for each system were obtained using the methods described in (*32*).

Hydrogen bond quality index analyses

We employed our hydrogen bond quality index (HBI) (*13, 40*), to quantitatively assess the quality of Watson-Crick hydrogen bonding, in terms of the deviation from ideal Watson-Crick hydrogen bond distances and angles:

$$I_H = \sum_{Snapshot} \sum_{D-H...A} [(d_{DA} - d_{DA}^0)^2 + (1 + \cos\gamma)^2]$$

where d_{DA} is the instantaneous donor-acceptor distance, d_{DA}^0 is an ideal donor-acceptor distance (*41*) [for G:C pair: O6 (G) to N4 (C) is 2.91 Å, N1 (G) to N3 (C) is 2.95 Å, and N2 (G) to O2 (C) is 2.86 Å; for A:T pair: N (A) to O4 (T) is 2.95 Å, and N1 (A) to N (T) is 2.82 Å] and γ is the instantaneous donor-hydrogen···acceptor (D-H···A) hydrogen bond angle with an ideal value of 180 °. The summation is over all the Watson-Crick hydrogen bonds in a base pair over the trajectory. Snapshots were selected at 10 ps intervals over the 20-65 ns of the trajectory and 4500 snapshots were used. The lower the value of I_H, the better the quality of the Watson-Crick hydrogen bonding. I_H is zero when the Watson-Crick hydrogen bonding is ideal during the dynamics. However, in real, even unmodified DNA, sequence-dependent

deviations from ideal Watson-Crick hydrogen bonding are normal (*42*). Comparing the I_H value of a modified step to its analogue step in the unmodified control duplex provides an estimate of the integrity of its Watson-Crick hydrogen bond upon modification.

Modeling and computational resources

The INSIGHT II 2005 program (Accelrys Software, Inc.) was employed to visualize and build models. PyMOL (Delano Scientific, LLC.) (*43*) was employed to make molecular images and movies. Computations were carried out on our own cluster of Silicon Graphic Origin and Altix high-performance computers and through TeraGrid resources TG-MCB060028N at the Texas Advanced Computing Center provided by the National Science Foundation.

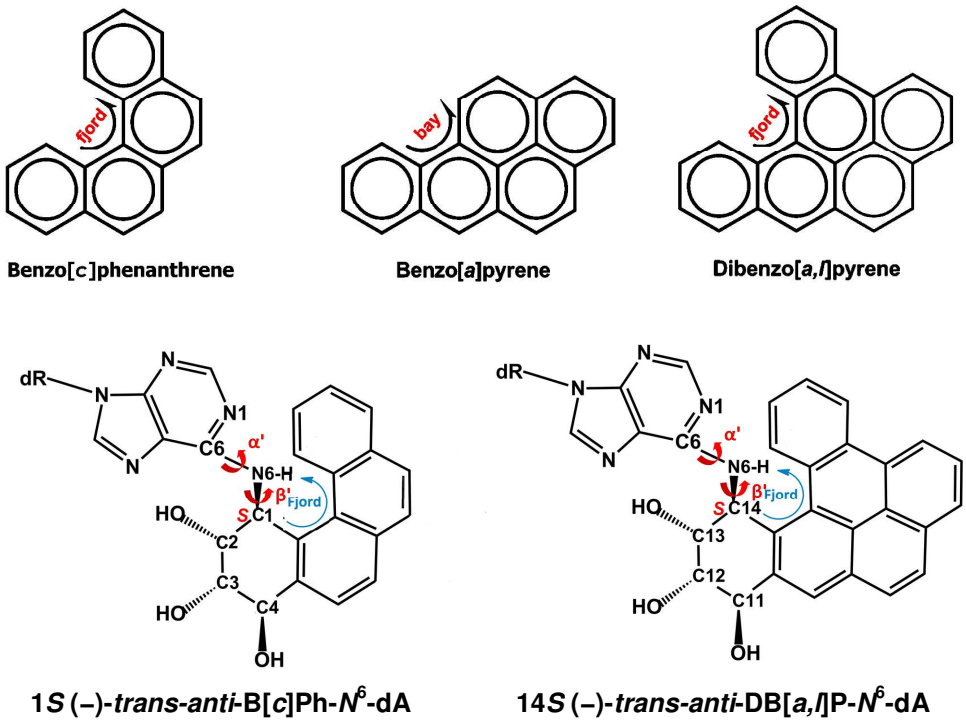

Figure S1. Chemical structures of B[*c*]Ph, B[*a*]P, DB[*a,l*]P, the 1*S* (–)-*trans-anti*-B[*c*]Ph-N^6-dA adduct and the 14*S* (–)-*trans-anti*-DB[*a,l*]P-N^6-dA adduct with designation of fjord and bay regions. The DB[*a,l*]P adduct was built from the B[*c*]Ph by adding two rings. The lesion-DNA linkage site torsion angles α´ and β´ are defined as follows: α´, N1-C6-*N*-C1 (B[*c*]Ph); β´, C6-*N*-C1 (B[*c*]Ph)-C2 (B[*c*]Ph) for the 1*S* (–)-*trans-anti*-B[*c*]Ph-N^6-dA adduct; and α´, N1-C6-*N*-C14(DB[*a,l*]P); β´, C6-*N*-C14(DB[*a,l*]P)-C13(DB[*a,l*]P) for the 14*S* (–)-*trans-anti*-DB[*a,l*]P-N^6-dA adduct.

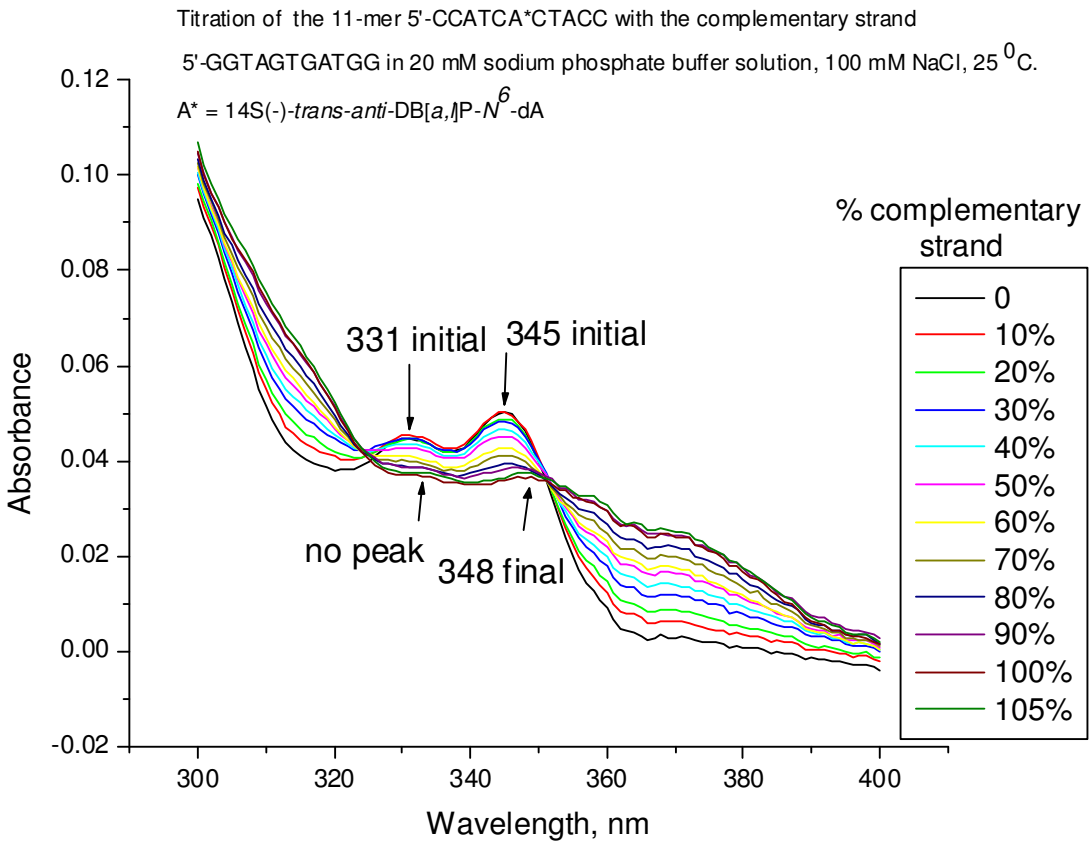

Figure S2. Titration of the DB[*a,l*]P diol epoxide-modified strand containing a single 14*S* (−)-*trans*-*anti*-DB[*a,l*]P-N^6-dA adduct with the complementary unmodified strand. The red-shifted absorption spectra in the double-stranded DNA molecules are characteristic of intercalative adduct conformations. The broadened red-shifted absorption spectra reveal that there is a significant heterogeneity in the base-stacking interactions in these double-stranded duplexes (Cai Y. , Broyde S., manuscript in preparation).

Background. As shown earlier (*44, 45*), intercalated benzo[*a*]pyrene-derived DNA lesions are characterized by red-shifted UV absorption spectra relative to the absorption spectra of the same PAH residue in single-stranded DNA. External minor groove adduct conformations, on the other hand, are characterized by blue shifted spectra. These differences are revealed by titrating the PAH-modified single-stranded oligonucleotides with the complementary strand and observing the shifts in the absorption maxima as the double-stranded molecules are formed.

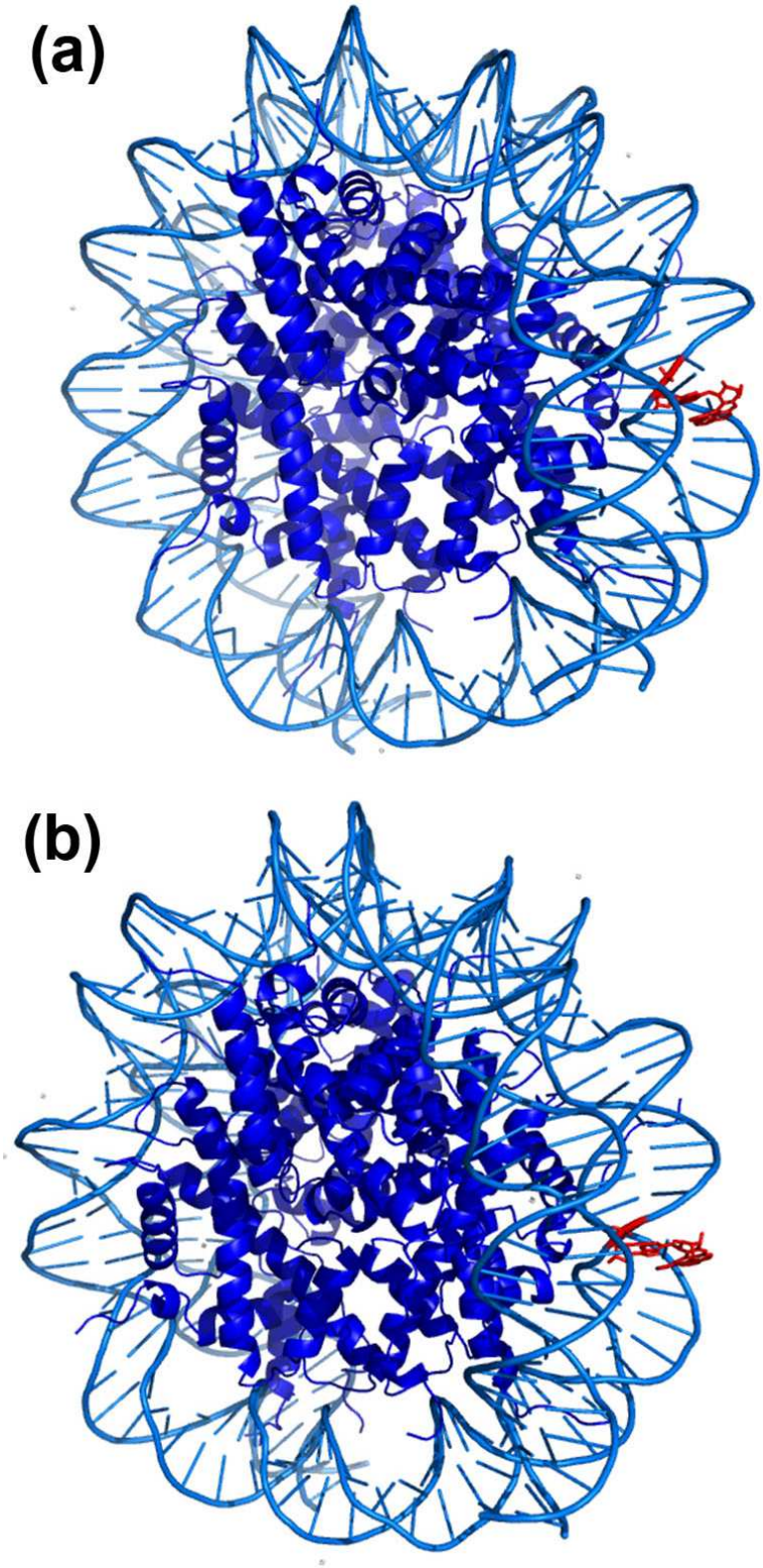

Figure S3. (a) Initial structure of the nucleosome core particle containing the 14*S* (–)-*trans*-*anti*-DB[*a,l*]P-N^6-dA lesion (red) and (b) Following 65-ns.

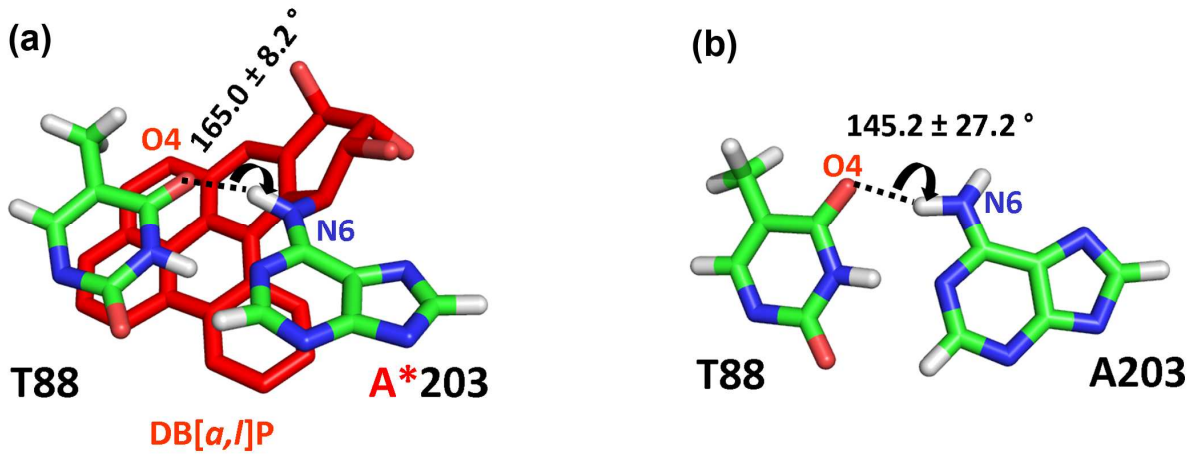

Figure S4. Views down the helix axis showing the more distorted hydrogen bond angle in the unmodified NCP compared to the modified one (See Table S2). Stacking of the DB[*a,l*]P ring system with the T88 partner base stabilizes this hydrogen bond angle.

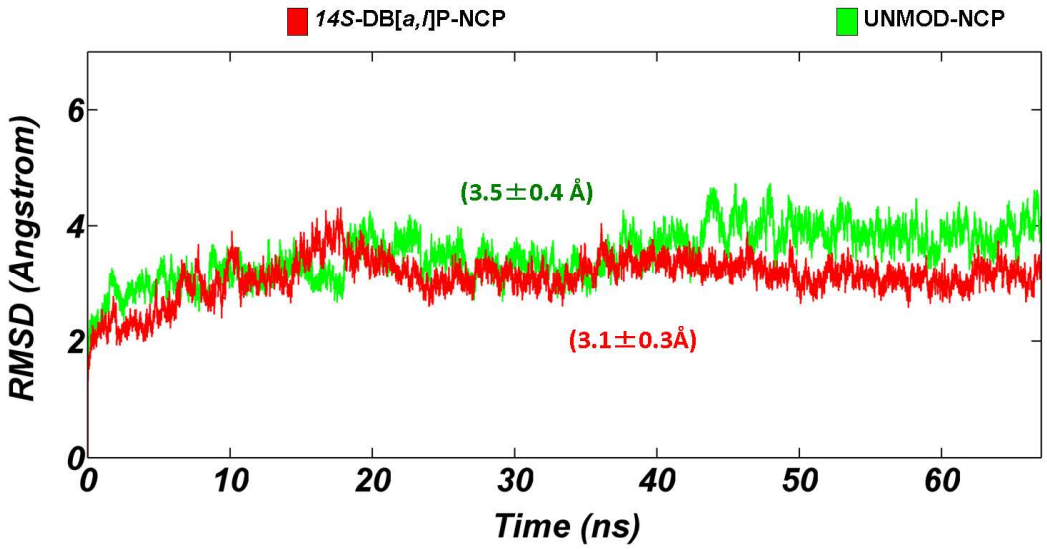

Figure S5. Time dependence of RMSDs for the entire NCP containing the 14*S* (–)-*trans*-*anti*-DB[*a,l*]P-N^6-dA adduct (red) and the entire unmodified NCP (green). The RMSDs were calculated relative to their respective initial structures. Only the solute (DNA and protein) was considered. The ensemble average RMSDs with standard deviations are given.

Table S1. Ensemble average van der Waals stacking interaction energies (kcal/mol) between adjacent base pairs and between the DB[*a,l*]P aromatic rings and surrounding bases in the interaction pocket for the damaged NCP, and between the analogous base pairs in the unmodified NCP. [a]

	14*S*-DB[*a,l*]P-NCP	**UNMOD-NCP**
A203:T88 -C204:G87	−2.3 (0.6)	−13.0 (1.7)
DB[*a,l*]P-intercalation pocket	−18.0 (2.2)	
DB[*a,l*]P-A203	−2.4 (1.8)	
DB[*a,l*]P-T88	−9.4 (0.7)	
DB[*a,l*]P-C204	−1.6 (0.5)	
DB[*a,l*]P-G87	−4.6 (1.0)	
Total	**−20.3 (2.2)**	**−13.0 (1.7)**

[a] Standard deviations are given in parentheses. The van der Waals stacking interaction energies between DB[*a,l*]P and partner T88 to the damaged A203 is highlighted in yellow.

Table S2. Ensemble average hydrogen bond distances and angles at the damaged base pair and the analogous base pair in the unmodified NCP [a]

		14*S*-DB[*a*,*l*]P-NCP	UNMOD-NCP
HB Angles (°)	N6-H61…O4	165.0 (8.2)	145.2 (27.2)
	N3-H3…N1	163.7 (8.4)	161.1 (12.6)
HB Distances (Å)	N6…O4	3.1 (0.2)	3.1 (0.4)
	N3…N1	3.0 (0.1)	3.0 (0.1)

[a] Standard deviations are given in parentheses. Hydrogen bond angles in ideal B-DNA are 180 °. Highlighted in yellow is the hydrogen bond angle that is more ideal in the lesion-containing NCP than in the unmodified NCP. Also note that the standard deviations for all angles are greater in the unmodified.

Table S3. Hydrogen bond occupancies between histone amino acid residues and DNA within 15 Å of the damaged residue A203* in the damaged NCP or A203 in the unmodified NCP.[a]

14*S*-DB[*a,l*]P-NCP			UNMOD-NCP		
Donor	Acceptor	Occup-ancies	Donor	Acceptor	Occup-ancies
Arg 702 (NH2)	T90 (O2P)	85 %			
Arg 702 (NE)	T90 (O2P)	70 %			
Arg 696 (NH2)	T90 (O3')	53 %			
Arg 696 (NE)	T90 (O3')	26 %			
Arg 696 (NH1)	C205 (O1P)	40 %	Arg 696 (NH2)	C205 (O2P)	50 %
Arg 696 (NE)	C205 (O1P)	7 %	Arg 696 (NE)	C205 (O1P)	83 %
Arg 696 (NE)	C204 (O3')	6 %	Arg 696 (NE)	C204 (O3')	43 %
Leu 698 (N)	T91 (O2P)	100 %	Leu 698 (N)	T91 (O2P)	100 %
Lys 697 (N)	T91 (O1P)	65 %	Lys 697 (N)	T91 (O1P)	89 %
Arg 788 (NH1)	C205 (O1P)	7 %	Arg 788 (NH2)	C205 (O1P)	80 %
Arg 788 (NH1)	C205 (O2P)	95 %	Arg 788 (NH1)	C205 (O2P)	82 %
Arg 788 (NH2)	C205 (O1P)	95 %	Arg 788 (NH2)	C205 (O1P)	20 %

[a] Criteria for hydrogen bonding: heavy atom-heavy atom distance < 3.3 Å, and donor-hydrogen-acceptor angle > 140 °. Note the hydrogen bonds (highlighted in yellow) in the 14*S*-DB[*a,l*]P-NCP involving Arg 702 which are not present in the unmodified NCP. All other hydrogen bond differences provide no net gain in total hydrogen bonds in the 14*S*-DB[*a,l*]P-NCP compared to the unmodified NCP. This can be seen by adding the occupancies for the two cases: 650 %, and 550 %, (or 6.5 and 5.5 hydrogen bonds) respectively, for the 14*S*-DB[*a,l*]P-NCP and unmodified NCP.

Table S4. Ensemble average groove widths (Å). [a] **Standard deviations are given in parentheses.**

Major groove width	14*S*-DB[*a*,*l*]P-NCP	Unmodified
P83-P205	10.5 ± 0.8	12.0 ± 0.8
P84-P204	10.3 ± 1.1	11.1 ± 1.4
P85-P203	15.8 ± 1.3	14.9 ± 1.8
P86-P202	18.2 ± 1.7	16.9 ± 2.0
P87-P201	18.9 ± 1.5	16.1 ± 2.2
P88-P200	15.9 ± 1.6	14.5 ± 1.5

Minor groove width	14*S*-DB[*a*,*l*]P-NCP	Unmodified
P86-P209	7.1 ± 1.3	6.7 ± 1.3
P87-P208	6.4 ± 1.3	6.2 ± 1.4
P88-P209	4.6 ± 1.2	3.8 ± 1.1
P89-P210	2.8 ± 1.2	3.0 ± 1.3
P90-P211	4.3 ± 0.8	3.1 ± 0.6
P91-P212	5.0 ± 0.8	4.3 ± 0.8
P92-P213	4.3 ± 1.5	3.9 ± 1.1

[a]The lesion site and its analogous site in the unmodified NCP are highlighted in yellow. Note the sharp minor groove narrowing in the damaged NCP (see also Figure 3c). The major groove opening in the damaged compared to the unmodified NCP stems from the intercalation on the major groove side.

Table S5. Partial charges, atom types and topologies for the 14*S* (–)-*trans*-*anti*-DB[*a,l*]P-N^6-dA adduct.

	Atom Name	Atom Type	Topology	Partial Charge
1	P	P	M	1.2687
2	O1P	O2	E	–0.795
3	O2P	O2	E	–0.795
4	O5'	OS	M	–0.476
5	C5'	CT	M	–0.169
6	H5'1	H1	E	0.1079
7	H5'2	H1	E	0.1079
8	C4'	CT	M	0.3142
9	H4'	H1	E	0.0639
10	O4'	OS	S	–0.451
11	C1'	CT	B	0.2203
12	H1'	H2	E	0.1191
13	N9	N*	S	–0.081
14	C8	CK	B	0.1243
15	H8	H5	E	0.1856
16	N7	NB	S	–0.661
17	C5	CB	S	0.0524
18	C6	CA	B	0.4648
19	N	N2	B	–0.535
20	HN	H	E	0.3617
21	C14	CT	B	–0.025
22	HC14	H1	E	0.1766
23	C13	CT	3	0.0299
24	HC13	H1	E	0.1574
25	O13	OH	S	–0.625
26	HO13	HO	E	0.3875
27	C12	CT	3	0.2376
28	HC12	H1	E	0.0834
29	O12	OH	S	–0.659
30	HO12	HO	E	0.4245
31	C11	CT	3	0.1874
32	HC11	H1	E	0.0222
33	O11	OH	S	–0.637
34	HO11	HO	E	0.4095
35	C16	CA	S	–0.019

36	C10	CA	B	−0.11
37	HC10	HA	E	0.134
38	C17	CA	B	0.0099
39	C18	CA	E	0.0406
40	C9	CA	B	−0.192
41	HC9	HA	E	0.1575
42	C8	CA	B	−0.216
43	HC8	HA	E	0.1477
44	C20	CA	B	0.0808
45	C21	CA	E	0.1306
46	C7	CA	B	−0.209
47	HC7	HA	E	0.1559
48	C6	CA	B	−0.207
49	HC6	HA	E	0.1425
50	C5	CA	B	−0.155
51	HC5	HA	E	0.1894
52	C22	CA	S	0.0278
53	C23	CA	S	0.0635
54	C4	CA	B	−0.217
55	HC4	HA	E	0.1477
56	C3	CA	B	−0.146
57	HC3	HA	E	0.1399
58	C2	CA	B	−0.146
59	HC2	HA	E	0.1255
60	C1	CA	B	−0.18
61	HC1	HA	E	0.1492
62	C24	CA	S	0.0454
63	C19	CA	S	−0.087
64	C15	CA	E	−0.062
65	N1	NC	S	−0.702
66	C2	CQ	B	0.6403
67	H2	H5	E	0.0355
68	N3	NC	S	−0.787
69	C4	CB	E	0.4804
70	C3'	CT	M	0.2263
71	H3'	H1	E	0.0398
72	C2'	CT	B	−0.056
73	H2'1	HC	E	0.0257
74	H2'2	HC	E	0.0257
75	O3'	OS	M	−0.467

Table S6. Added force field parameters [a]

Angle	K_θ (kcal·mol^{-1}·rad^{-2})	θ_{eq} (deg)
N2-CT-CA	80.0	111.20
H1-CT-CA	50.0	109.50
OH-CT-CA	50.0	109.50

[a] Missing bond and angle parameters were added to the force field by analogy to chemically similar atom types already exist in the parm99 parameter set.

References

1. Berman, H. M., Westbrook, J., Feng, Z., Gilliland, G., Bhat, T. N., Weissig, H., Shindyalov, I. N., and Bourne, P. E. (2000) The Protein Data Bank, *Nucleic Acids Res. 28*, 235-242.
2. Ong, M. S., Richmond, T. J., and Davey, C. A. (2007) DNA stretching and extreme kinking in the nucleosome core, *J. Mol. Biol. 368*, 1067-1074.
3. Davey, G. E., Wu, B., Dong, Y., Surana, U., and Davey, C. A. (2010) DNA stretching in the nucleosome facilitates alkylation by an intercalating antitumour agent, *Nucleic Acids Res. 38*, 2081-2088.
4. Buterin, T., Hess, M. T., Luneva, N., Geacintov, N. E., Amin, S., Kroth, H., Seidel, A., and Naegeli, H. (2000) Unrepaired fjord region polycyclic aromatic hydrocarbon-DNA adducts in ras codon 61 mutational hot spots, *Cancer Res. 60*, 1849-1856.
5. Cosman, M., Fiala, R., Hingerty, B. E., Laryea, A., Lee, H., Harvey, R. G., Amin, S., Geacintov, N. E., Broyde, S., and Patel, D. (1993) Solution conformation of the (+)-*trans-anti*-[BPh]dA adduct opposite dT in a DNA duplex: intercalation of the covalently attached benzo[*c*]phenanthrene to the 5'-side of the adduct site without disruption of the modified base pair, *Biochemistry 32*, 12488-12497.
6. Cosman, M., Laryea, A., Fiala, R., Hingerty, B. E., Amin, S., Geacintov, N. E., Broyde, S., and Patel, D. J. (1995) Solution conformation of the (–)-*trans-anti*-benzo[*c*]phenanthrene-dA ([BPh]dA) adduct opposite dT in a DNA duplex: intercalation of the covalently attached benzo[*c*]phenanthrenyl ring to the 3'-side of the adduct site and comparison with the (+)-*trans-anti*-[BPh]dA opposite dT stereoisomer, *Biochemistry 34*, 1295-1307.
7. Yan, S., Wu, M., Buterin, T., Naegeli, H., Geacintov, N. E., and Broyde, S. (2003) Role of base sequence context in conformational equilibria and nucleotide excision repair of benzo[*a*]pyrene diol epoxide-adenine adducts, *Biochemistry 42*, 2339-2354.
8. Suri, A. K., Mao, B., Amin, S., Geacintov, N. E., and Patel, D. J. (1999) Solution conformation of the (+)-*trans-anti*-benzo[g]chrysene-dA adduct opposite dT in a DNA duplex, *J Mol Biol 292*, 289-307.
9. Ruan, Q., Kolbanovskiy, A., Zhuang, P., Chen, J., Krzeminski, J., Amin, S., and Geacintov, N. E. (2002) Synthesis and characterization of site-specific and stereoisomeric fjord dibenzo[a,l]pyrene diol epoxide-N(6)-adenine adducts: unusual thermal stabilization of modified DNA duplexes, *Chem Res Toxicol 15*, 249-261.
10. Mao, B., Gu, Z., Gorin, A., Chen, J., Hingerty, B. E., Amin, S., Broyde, S., Geacintov, N. E., and Patel, D. J. (1999) Solution structure of the (+)-cis-anti-benzo[a]pyrene-dA ([BP]dA) adduct opposite dT in a DNA duplex, *Biochemistry 38*, 10831-10842.
11. Schurter, E. J., Yeh, H. J., Sayer, J. M., Lakshman, M. K., Yagi, H., Jerina, D. M., and Gorenstein, D. G. (1995) NMR solution structure of a nonanucleotide duplex with a dG mismatch opposite a 10R adduct derived from trans addition of a deoxyadenosine N6-amino group to (-)-(7S,8R,9R,10S)-7,8-dihydroxy-9,10-epoxy-7,8,9,10- tetrahydrobenzo[a]pyrene, *Biochemistry 34*, 1364-1375.
12. Schwartz, J. L., Rice, J. S., Luxon, B. A., Sayer, J. M., Xie, G., Yeh, H. J., Liu, X., Jerina, D. M., and Gorenstein, D. G. (1997) Solution structure of the minor conformer of a DNA duplex containing a dG mismatch opposite a benzo[a]pyrene diol epoxide/dA adduct: glycosidic rotation from syn to anti at the modified deoxyadenosine, *Biochemistry 36*, 11069-11076.
13. Yan, S., Shapiro, R., Geacintov, N. E., and Broyde, S. (2001) Stereochemical, structural, and thermodynamic origins of stability differences between stereoisomeric benzo[*a*]pyrene diol epoxide deoxyadenosine adducts in a DNA mutational hot spot sequence, *J. Am. Chem. Soc. 123*, 7054-7066.
14. Yeh, H. J., Sayer, J. M., Liu, X., Altieri, A. S., Byrd, R. A., Lakshman, M. K., Yagi, H., Schurter, E. J., Gorenstein, D. G., and Jerina, D. M. (1995) NMR solution structure of a nonanucleotide duplex with a dG mismatch opposite a 10*S* adduct derived from trans addition of a deoxyadenosine N^6-amino group to (+)-(7*R*,8*S*,9*S*,10*R*)-7,8-dihydroxy-9,10-epoxy-7,8,9,10- tetrahydrobenzo[*a*]pyrene: an unusual *syn* glycosidic torsion angle at the modified dA, *Biochemistry 34*, 13570-13581.

15. Zegar, I. S., Chary, P., Jabil, R. J., Tamura, P. J., Johansen, T. N., Lloyd, R. S., Harris, C. M., Harris, T. M., and Stone, M. P. (1998) Multiple conformations of an intercalated (-)-(7S,8R,9S, 10R)-N6-[10-(7,8,9,10-tetrahydrobenzo[a]pyrenyl)]-2'-deoxyadenosyl adduct in the N-ras codon 61 sequence, *Biochemistry 37*, 16516-16528.
16. Zegar, I. S., Kim, S. J., Johansen, T. N., Horton, P. J., Harris, C. M., Harris, T. M., and Stone, M. P. (1996) Adduction of the human N-ras codon 61 sequence with (-)-(7S,8R,9R,10S)-7,8-dihydroxy-9,10-epoxy-7,8,9,10-tetrahydrobenzo[a] pyrene: structural refinement of the intercalated SRSR(61,2) (-)-(7S,8R,9S,10R)-N6-[10-(7,8,9,10- tetrahydrobenzo[a]pyrenyl)]-2'-deoxyadenosyl adduct from 1H NMR, *Biochemistry 35*, 6212-6224.
17. Wu, M., Yan, S., Patel, D. J., Geacintov, N. E., and Broyde, S. (2002) Relating repair susceptibility of carcinogen-damaged DNA with structural distortion and thermodynamic stability, *Nucleic Acids Res. 30*, 3422-3432.
18. Frisch J.M., Trucks W.G., Schlegel B.H., Scuseria E.G., Robb A.M., Cheeseman R.J., Zakrzewski G.V., Montgomery A.J., Stratmann E.R., Burant C.J., Dappprich S., Millam M.J., Daniels D.A., Kudin N.K., Strain C.M., Farkas O., Tomasi J., Barone V., Cossi M., Cammi R., Mennucci B., Pomelli C., Adamo C., Clifford, S., Ochterski J., Petersson A.G., Ayala Y.P., Cui Q., Morokuma K., Malick K.D., Rabuck D.A., Raghavachari K., Foresman B.J., Cioslowski J., Ortiz V.J., Baboul G.A., Stefanov B.B., Liu G., Liashenko A., Piskorz P., Komaromi I., Comperts R., Martin L.R., Fox J.D., Keith T., Al-Laham A.M., Peng Y.C., Nanayakkara A., Gonzalez C., Challacombe M., Gill W.M.P., Johnson, B., Chen W., Wong W.M., Andres L.J., Head-Gordon M., Replogle S.E., and Pople A.J. (1998) Gaussian 98, Gaussian, Inc., Pittsburgh.
19. Simmerling, C., Elber, R., and Zhang, J. (1995) MOIL-View –A program for visualization of structure and dynamics of biomolecules and STO–A program for computing stochastic paths, in modeling of biomolecular structure and mechanisms, (Pullman, A., Ed.), Kluwer, Netherlands.
20. Cieplak, P., Cornell, W. D., Bayly, C., and Kollman, P. A. (1995) Application of the multimolecule and multiconformational Resp methodology to biopolymers - Charge derivation for DNA, RNA, and proteins, *J. Comput. Chem. 16*, 1357-1377.
21. Hornak, V., Abel, R., Okur, A., Strockbine, B., Roitberg, A., and Simmerling, C. (2006) Comparison of multiple Amber force fields and development of improved protein backbone parameters, *Proteins 65*, 712-725.
22. Wang, J. M., Cieplak, P., and Kollman, P. A. (2000) How well does a restrained electrostatic potential (RESP) model perform in calculating conformational energies of organic and biological molecules?, *J. Comput. Chem. 21*, 1049-1074.
23. Cheatham, T. E., Cieplak, P., and Kollman, P. A. (1999) A modified version of the Cornell et al. force field with improved sugar pucker phases and helical repeat, *J. Biomol. Struct. Dyn. 16*, 845-862.
24. Perez, A., Marchan, I., Svozil, D., Sponer, J., Cheatham, T. E., 3rd, Laughton, C. A., and Orozco, M. (2007) Refinement of the AMBER force field for nucleic acids: improving the description of alpha/gamma conformers, *Biophys J 92*, 3817-3829.
25. Bayly, C. I., Cieplak, P., Cornell, W. D., and Kollman, P. A. (1993) A well-behaved electrostatic potential based method using charge restraints for deriving atomic charges - the Resp model, *J. Phys. Chem.-Us 97*, 10269-10280.
26. Cieplak, P., Cornell, W. D., Bayly, C., and Kollman, P. A. (1995) Application of the multimolecule and multiconformational Resp methodology to biopolymers - Charge derivation for DNA, RNA, and proteins, *J. Comput. Chem. 16*, 1357-1377.
27. Dolinsky, T. J., Czodrowski, P., Li, H., Nielsen, J. E., Jensen, J. H., Klebe, G., and Baker, N. A. (2007) PDB2PQR: expanding and upgrading automated preparation of biomolecular structures for molecular simulations, *Nucleic Acids Res 35*, W522-525.
28. Dolinsky, T. J., Nielsen, J. E., McCammon, J. A., and Baker, N. A. (2004) PDB2PQR: an automated pipeline for the setup of Poisson-Boltzmann electrostatics calculations, *Nucleic Acids Res 32*, W665-667.
29. Case, D. A., Darden, T. A., Cheatham III, T. E., Simmerling, C. L., Wang, J., Duke, R. E., Luo, R., Merz, K. M., Pearlman, D. A., Crowley, M., Walker, R. C., Zhang, W., Wang, B., Hayik, S., Roitberg, A., Seabra, G., Wong, K. F., Paesani, F., Wu, X., Brozell, S., Tsui, V., Gohlke, H., Yang, L., Tan, C., Mongan, J., Hornak, V., Cui, G., Beroza, P., Mathews, D. H.,

Schafmeister, C., Ross, W. S., and Kollman, P. A. (2006) AMBER 9, University of California, San Francisco, CA.
30. Mezei, M. (1997) Optimal position of the solute for simulations., *J. Comp. Chem. 18*, 812-815.
31. Jorgensen, W. L., Chandreskhar, J., Madura, J. D., Imprey, R. W., and Klein, M. L. (1983) Comparison of simple potential functions for simulating liquid water, *J. Chem. Phys. 79*, 926-935.
32. Donny-Clark, K., and Broyde, S. (2009) Influence of local sequence context on damaged base conformation in human DNA polymerase iota: molecular dynamics studies of nucleotide incorporation opposite a benzo[a]pyrene-derived adenine lesion, *Nucleic Acids Res 37*, 7095-7109.
33. Darden, T., York, D., and Pedersen, L. (1993) Particle mesh Ewald: an *N* log(*N*) method for Ewald sums in large systems, *J. Chem. Phys. 98*, 10089-10092.
34. Essmann, U., Perera, L., Berkowitz, M. L., Darden, T., Lee, H., and Pederson, L. G. (1995) A smooth particle mesh Ewald method, *J. Chem. Phys. 103*, 8577-8593.
35. Ryckaert, J. P., Ciccotti, G., and Berendsen, H. J. C. (1977) Numerical integration of cartesian equations of motion of a system with constraints: molecular dynamics of *n*-alkanes, *J. Comp. Phys. 23*, 327-341.
36. Case, D. A., Pearlman, D. A., Caldwell, J. W., Cheatham III, T. E., Wang, J., Ross, W. S., Simmerling, C. L., Darden, T. A., Merz, K. M., Stanton, R. V., Cheng, A. L., Vincent, J. J., Crowley, M., Tsui, V., Gohlke, H., Radmer, R. J., Duan, Y., Pitera, J., Massova, I., Seibel, G. L., Singh, U. C., Weiner, P. K., and Kollman, P. A. (2002) AMBER 7, University of California, San Francisco, CA.
37. Ravishanker, G., and Beveridge, D. L. (1993) MD Toolchest 2.0, Wesleyan University, Middletown, CT 06459.
38. Ravishanker, G., Swaminathan, S., Beveridge, D. L., Lavery, R., and Sklenar, H. (1989) Conformational and helicoidal analysis of 30 ps of molecular dynamics on the d(CGCGAATTCGCG) double helix: "curves", dials and windows, *J. Biomol. Struct. Dyn. 6*, 669-699.
39. Fratini, A. V., Kopka, M. L., Drew, H. R., and Dickerson, R. E. (1982) Reversible bending and helix geometry in a B-DNA dodecamer: CGCGAATTBrCGCG, *J. Biol. Chem. 257*, 14686-14707.
40. Hingerty, B. E., Figueroa, S., Hayden, T. L., and Broyde, S. (1989) Prediction of DNA structure from sequence: a build-up technique, *Biopolymers 28*, 1195-1222.
41. Saenger, W. (1983) Polymorphism of DNA, in *Principles of Nucleic Acid Structure* p226, Springer-Verlag, New York.
42. Calladine, C. R., and Drew, H. R. (1997) *Understanding DNA: The Molecule and How it Works*, Morgan Kaufmann.
43. DeLano, W. L. (2002) The PyMOL Molecular Graphics System, DeLano Scientific, Palo Alto, CA, USA.
44. Huang, W., Amin, S., and Geacintov, N. E. (2002) Fluorescence characteristics of site-specific and stereochemically distinct benzo[*a*]pyrene diol epoxide-DNA adducts as probes of adduct conformation., *Chem. Res. Toxicol. 15*, 118-126.
45. Huang, X., Colgate, K. C., A., K., S., A., and N.E., G. (2002) Conformational changes of a benzo[a]pyrene diol epoxide-N(2)-dG adduct induced by a 5'-flanking 5-methyl-substituted cytosine in a (Me)CG double-stranded oligonucleotide sequence context., *Chem. Res. Toxicol. 15*, 438-444.